DOI: 10.1002/cssc.201402361

Effect of Preparation Method and CuO Promotion in the Conversion of Ethanol into 1,3-Butadiene over SiO_2–MgO Catalysts

Carlo Angelici, Marjolein E. Z. Velthoen, Bert M. Weckhuysen,* and Pieter C. A. Bruijnincx*[a]

Silica–magnesia (Si/Mg = 1:1) catalysts were studied in the one-pot conversion of ethanol to butadiene. The catalyst synthesis method was found to greatly influence morphology and performance, with materials prepared through wet-kneading performing best both in terms of ethanol conversion and butadiene yield. Detailed characterization of the catalysts synthesized through co-precipitation or wet-kneading allowed correlation of activity and selectivity with morphology, textural properties, crystallinity, and acidity/basicity. The higher yields achieved with the wet-kneaded catalysts were attributed to a morphology consisting of SiO_2 spheres embedded in a thin layer of MgO. The particle size of the SiO_2 catalysts also influenced performance, with catalysts with smaller SiO_2 spheres showing higher activity. Temperature-programmed desorption (TPD) measurements showed that best butadiene yields were obtained with SiO_2–MgO catalysts characterized by an intermediate amount of acidic and basic sites. A Hammett indicator study showed the catalysts' pK_a value to be inversely correlated with the amount of dehydration by-products formed. Butadiene yields could be further improved by the addition of 1 wt% of CuO as promoter to give butadiene yields and selectivities as high as 40% and 53%, respectively. The copper promoter boosts the production of the acetaldehyde intermediate changing the rate-determining step of the process. TEM-energy-dispersive X-ray (EDX) analyses showed CuO to be present on both the SiO_2 and MgO components. UV/Vis spectra of promoted catalysts in turn pointed at the presence of cluster-like CuO species, which are proposed to be responsible for the increased butadiene production.

Introduction

It has been advocated that future biorefineries need to produce high-value bio-based chemicals in addition to the lower-value biofuels to be economically competitive.[1] The production of 'drop-in' renewable chemicals, that is, direct, molecularly identical yet sustainably produced replacements for current petrochemical chemicals, is particularly attractive as efficient production routes can serve existing markets and make use of existing infrastructure.

Due to its (mandated) use as fuel and fuel additive, bioethanol is currently produced in increasingly large volumes, leading to decrease in ethanol market prices. Importantly, this future growth in bioethanol production is expected to mainly result from the utilization of 2nd or 3rd generation biomass.[2,3] The expected increased availability and shift to inedible feedstocks will ensure that low-cost ethanol will not only be available as fuel but also for the production of renewable bulk chemicals. Indeed, ethanol can serve as an excellent platform chemical, as many bulk chemicals currently are or can in principle be produced from ethanol.[1,4] The bulk chemical 1,3-butadiene (hereon simply called butadiene), which finds major application in the polymer industry, can for instance be produced from ethanol.

Butadiene is currently obtained as by-product of ethylene production in hydrocarbon steam cracking, with its isolation requiring a number of expensive extractive distillation steps.[5] The predicted shift towards lighter feeds for steam cracking, as a result of the recent shale gas boom, threatens butadiene production and is expected to significantly affect its price; efficient on-purpose production technologies for butadiene are, therefore, highly desirable.[6]

During the first decades of the twentieth century, two closely related processes were developed for the synthesis of butadiene from ethanol, that is, the Ostromisslenski[7] and Lebedev processes.[8,9] The first consists of two consecutive steps, that is, dehydrogenation of ethanol to acetaldehyde followed by condensation of acetaldehyde and ethanol to give butadiene; the Lebedev process, on the other hand, is a one-pot, one-step process used for direct butadiene synthesis from ethanol. The mechanism of this gas-phase conversion is complex and has not yet been unambiguously demonstrated. Most commonly a mechanistic pathway is proposed that involves consecutive dehydrogenation, aldol condensation, reduction and dehydration steps (see Scheme 1).[10] The ideal catalyst for this process thus requires a subtle balance of different active sites (acidic, basic, and redox) to be struck, both in terms of strength as well as number.

[a] C. Angelici, M. E. Z. Velthoen, Prof. B. M. Weckhuysen, Dr. P. C. A. Bruijnincx
Inorganic Chemistry and Catalysis
Debye Institute for Nanomaterials Science
Utrecht University
Universiteitsweg 99, 3584 CG Utrecht (The Netherlands)
E-mail: b.m.weckhuysen@uu.nl
p.c.a.bruijnincx@uu.nl

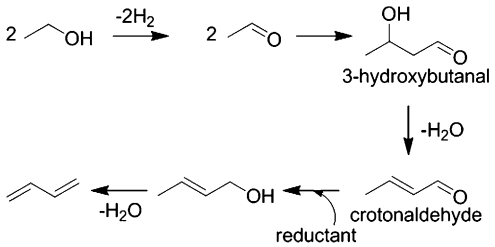

Scheme 1. Commonly proposed mechanism for the Lebedev conversion of ethanol into 1,3-butadiene.[10]

Different classes of catalysts (metal nanoparticles supported on clay materials, on oxides, or on mixed oxides) have been employed in the Lebedev process, and the catalytic aspects have been recently reviewed by us.[4] (Mixed) metal oxides have been studied most, with SiO_2–MgO systems, of different composition and obtained through different preparation procedures, often performing best in terms of butadiene yield.[11,12] It was previously shown that redox-active promoters can improve performance, considering that butadiene yields are typically lower than 20% with unpromoted SiO_2–MgO systems,[12,13] the only exception being the results reported by Ohnishi et al. (butadiene yield 42% at 623 K).[14] The same study showed a remarkable sensitivity of catalyst performance to impregnation of the SiO_2–MgO materials with 0.1 wt% of Na_2O and K_2O (leading to yields of 87 and 70%, respectively), thus implying that the balance of acidic and basic active sites is subtle yet critical for high activity and selectivity.[14] A recent publication by Jones et al. investigated for the first time the use of bi- and trimetallic systems supported on various metal oxides again pointing at the importance of using SiO_2.[15] Furthermore, a number of transition metals and metal oxides, such as CuO,[13,16] ZnO,[17] Cr_2O_3,[17] and NiO[18] were employed as promoters to improve the dehydrogenation activity of the catalyst and thus the final butadiene yield. In most cases, scarce details on catalyst structure, product distribution, and long-term activity were provided for the various catalysts tested; as a result the salient features of these (promoted) SiO_2–MgO catalysts are not yet fully understood.

Herein, we report on the activity of various SiO_2–MgO materials as catalysts for the Lebedev process. Different preparation methods were employed for the SiO_2–MgO catalysts with the aim of establishing a structure–activity relationship. The significant differences in terms of butadiene yield observed can indeed be correlated to structural differences, for example, in morphology, dispersion, and acid/base properties. It is also shown that CuO promotion on the SiO_2–MgO systems improves butadiene yield substantially in all cases. The nature of the supported CuO is also shown to have an important effect on catalysis.

Results and Discussion

Catalytic activity

Combinations of SiO_2 and MgO of different molar ratios have often been reported as promising catalysts for the Lebedev process.[11,12] Here, we study a series of six differently prepared SiO_2–MgO catalysts, having a nominal 1:1 molar ratio (see the Experimental Section).

The influence of preparation method on catalytic performance was studied using a physical mixture [PM, SiO_2–MgO (I)], three wet-kneaded catalysts [WK, SiO_2–MgO (II)–(IV)], and two co-precipitated ones [CP, SiO_2–MgO (V) and (VI)] (see Table 2 for details on the preparation methods). These samples show distinct differences in morphology (vide infra) and, as a result, high variability in catalytic activity. For these catalyst materials, activity and selectivity with 24 h on stream are reported (Figure 1), providing the first data on long-term catalyst performance in the Lebedev process. The physical mixture SiO_2–MgO (I) showed low ethanol conversion and butadiene yield. Catalytic testing of the two single oxides under identical conditions (data not shown) showed that SiO_2 was quite inert and gave negligible ethanol conversion and no butadiene, whereas the use of MgO resulted in low ethanol conversion and butadiene yield (1.7% after 4 h time on stream). Notably, the physical mixture SiO_2–MgO (I) showed a butadiene yield similar to pure MgO, again illustrating the inertness of isolated

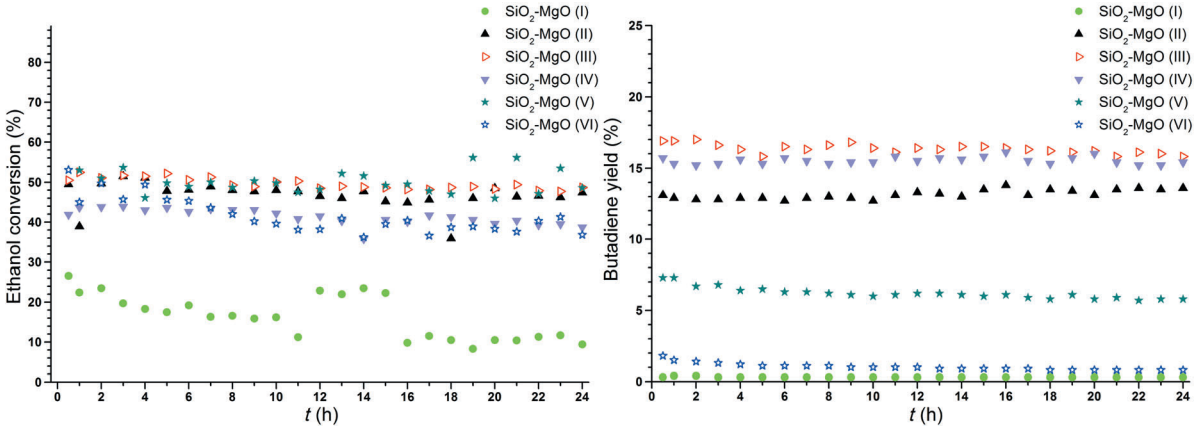

Figure 1. Ethanol conversion (left) and butadiene yield (right) as a function of time-on-stream over the different SiO_2–MgO catalysts tested. Conditions: 0.2 g catalyst, reaction temperature 698 K, ethanol (gas phase) and nitrogen flow 2 and 98 mL min^{-1}, respectively.

SiO_2. As expected, all chemically mixed SiO_2–MgO catalysts showed higher ethanol conversions and butadiene yields. The time on stream data furthermore shows that conversions and butadiene yields are stable in time (Figure 1) and no appreciable deactivation can be observed.

At similar conversion levels (50–65%), the catalysts showed significant differences in butadiene yield with performance increasing in the order: PM < CP < WK (Figure 1). The catalysts prepared by co-precipitation performed poorly, with almost negligible amounts of butadiene produced with SiO_2–MgO (VI) and a low, yet stable butadiene yield of approximately 6% for SiO_2–MgO (V). The catalysts prepared through wet-kneading [SiO_2–MgO (II)–(IV)] gave significantly higher butadiene yields. While SiO_2–MgO (II) showed the highest ethanol conversion, it gave the lowest butadiene yield of the wet-kneaded catalysts. SiO_2–MgO (III) performed best, yielding ~17% butadiene with 33% selectivity, even after 24 h time on stream. These differences in catalytic activity can be clearly related to differences in morphology and acidity/basicity of the materials, as shown below.

Not only the butadiene yield, but also the identity and number of by-products formed have a large influence on the ability of the Lebedev process to compete with traditional butadiene routes.[19] Indeed, as product separation is often costly, an ethanol conversion process that yields a limited number of products, which are in turn easily separable and individually can find a value-added application, is highly desired. Any ethylene produced can, for instance, be easily separated by distillation, whereas co-produced butenes would make separation of butadiene from the reaction mixture much more difficult.[5] Other compounds that can be present in the product stream are diethyl ether, higher alcohols and, of course, process intermediates such as acetaldehyde. To judge the efficiency of a process, it is, therefore, important that the whole product composition is reported, rather than just the butadiene yield. The product distributions for the six SiO_2–MgO catalysts at $t = 0.5$ and 4 h show considerable differences (Figure 2). Diethyl ether production, which is undesired as two ethanol molecules are consumed upon formation, is $\leq 5\%$ for all catalysts. On the other hand, substantial amounts of ethylene were observed, in particular over the two CP catalysts.

All WK catalysts, but particularly SiO_2–MgO (II), showed a much lower selectivity to ethylene and diethyl ether, suggesting that the CP catalysts are much more acidic than the WK ones. The amount of ethylene formed over the WK catalysts varied and, taken as a measure of acidity of the catalyst, could be correlated with SiO_2 particle size (see below).

Acetaldehyde, a key intermediate that can be formed by ethanol dehydrogenation on materials containing redox sites[20] but also on pure MgO,[21] is formed in too low amounts to allow any correlations to be made with catalyst structure. Although the mechanism depicted in Scheme 1 is generally accepted, different rate-determining steps have been proposed for butadiene production over SiO_2–MgO catalysts.[11,12,22] The fact that quite a low amount of acetaldehyde is observed for the SiO_2–MgO catalysts employed in this study might suggest that acetaldehyde formation is rate determining, as previously proposed by Niiyama et al.[11] Finally, various amounts of other components, identified to be mainly butenes, 1-butanol, and acetone, are formed over the different catalysts. SiO_2–MgO (II), for instance, produces a relatively large amount of others at the expense of ethylene and butadiene for which the yields are the lowest among the WK catalysts. Notably, SiO_2–MgO (IV) shows a remarkably low amount of other components, with ~90% of the products due to unconverted ethanol, ethylene, and butadiene. Finally, it should be noted that the combined yield of the different butenes (i.e., 1-butene, *cis*- and *trans*-2-butene), already discussed to be critical for purification of butadiene, is well below 5% in all cases.

CuO was added as promoter to the catalysts prepared through wet-kneading and co-precipitation. Different loadings (0.5, 1 and 2 wt%) as well as various thermal treatments (calcination in stagnant air, calcination in N_2 flow, and calcination in N_2 flow followed by reduction) were employed for CuO/SiO_2–MgO (II). The CuO loading did not have a strong effect on catalytic activity and selectivity; thermal treatment did matter and calcination in stagnant air provided the best catalyst (data not

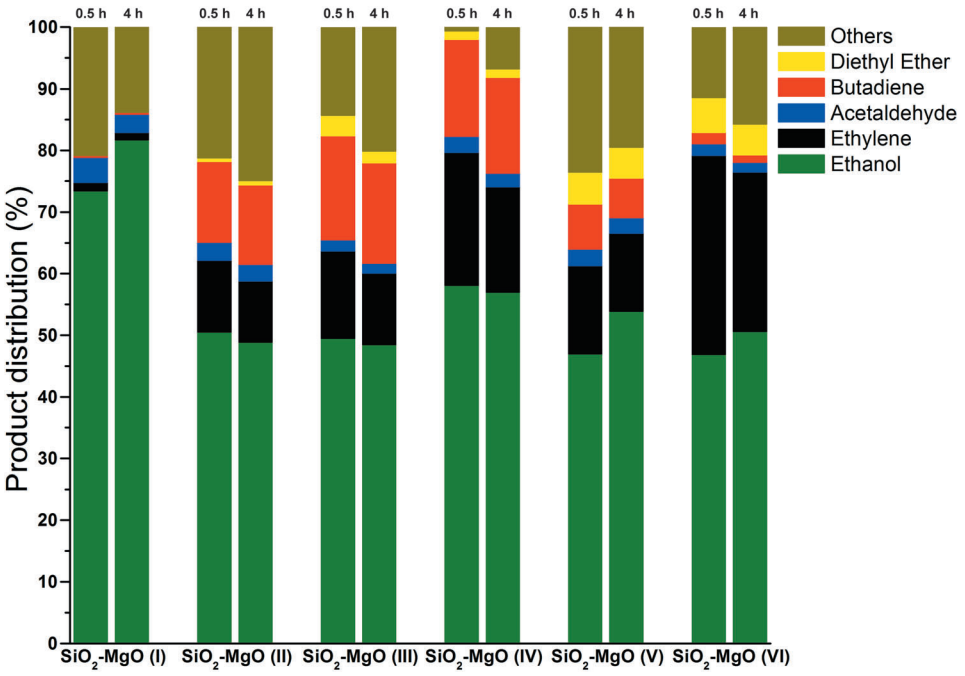

Figure 2. Product distribution for the different SiO_2–MgO catalysts after 0.5 and 4 h on stream. Conditions: 0.2 g catalyst, reaction temperature 698 K, ethanol (gas phase) and nitrogen flow 2 and 98 mL min^{-1}, respectively.

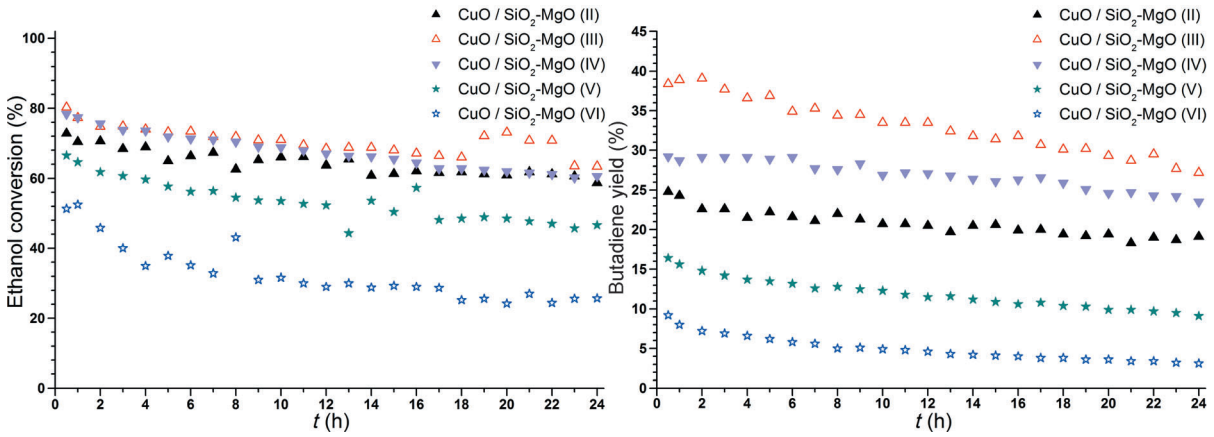

Figure 3. Ethanol conversion (left) and butadiene yield (right) as a function of time over the different CuO (1 wt%)/SiO_2–MgO catalysts tested. Conditions: 0.2 g catalyst, reaction temperature 698 K, ethanol (gas phase) and nitrogen flow 2 and 98 mL min^{-1}, respectively.

shown). Promotion of the WK SiO_2–MgO catalysts with CuO resulted in a strong increase in ethanol conversion, whereas the CuO-containing CP catalysts either showed a similar [CuO/SiO_2–MgO (V)] or reduced [CuO/SiO_2–MgO (VI)] conversion level (cf. Figure 1 and Figure 3). Most importantly, butadiene yield was strongly boosted upon addition of CuO: SiO_2–MgO catalysts show butadiene yields in the range 0.3–17% (selectivities 2–36%), whereas CuO-containing catalysts show 6–36% yields (selectivities 19–50%) after 4 h. Again, WK catalysts showed much higher yields than CP ones.

Wet-kneaded catalyst CuO/SiO_2–MgO (II) gave moderate but fairly stable butadiene yields of 23–28%. As with the non-CuO-containing catalysts, CuO/SiO_2–MgO (III) performed best with an initial yield of approximately 40%, corresponding to a butadiene selectivity of 53% (Table 1). In contrast to the unpromoted catalysts, the CuO-containing ones did show some deactivation, as evidenced by the gradual drop in ethanol conversion and butadiene yield with time on stream; the gradual deactivation can at least partially be ascribed to the increased amount of carbonaceous deposits that was detected for the promoted catalysts using UV/Vis analysis of the spent catalysts (data not shown).

Not only butadiene yield but also product distribution changed dramatically upon introduction of CuO (Figure 4). Notably, an increase in the amount of acetaldehyde produced was observed for all catalysts. The fact that butadiene and acetaldehyde yields increased simultaneously for the copper-promoted catalysts might be explained by considering that, for these catalysts, the rate-determining step is not the formation but rather the transformation of acetaldehyde, as proposed by Kvisle et al. for SiO_2–MgO systems.[12] Furthermore, the selectivity towards ethylene and diethyl ether is highly reduced in all cases. This suggests that CuO not only introduces redox-active sites, but also poisons the most acidic sites of the SiO_2–MgO samples. Alternatively, ethanol is preferentially dehydrogenated to acetaldehyde in the presence of CuO and, as a consequence, does not get a chance to undergo dehydration; given the incomplete ethanol conversion, the second hypothesis seems less likely. Finally, a substantial increase in the amount of other compounds formed was observed for the CuO-containing catalysts, especially with the WK samples. In addition to the previously observed butenes, 1-bu-

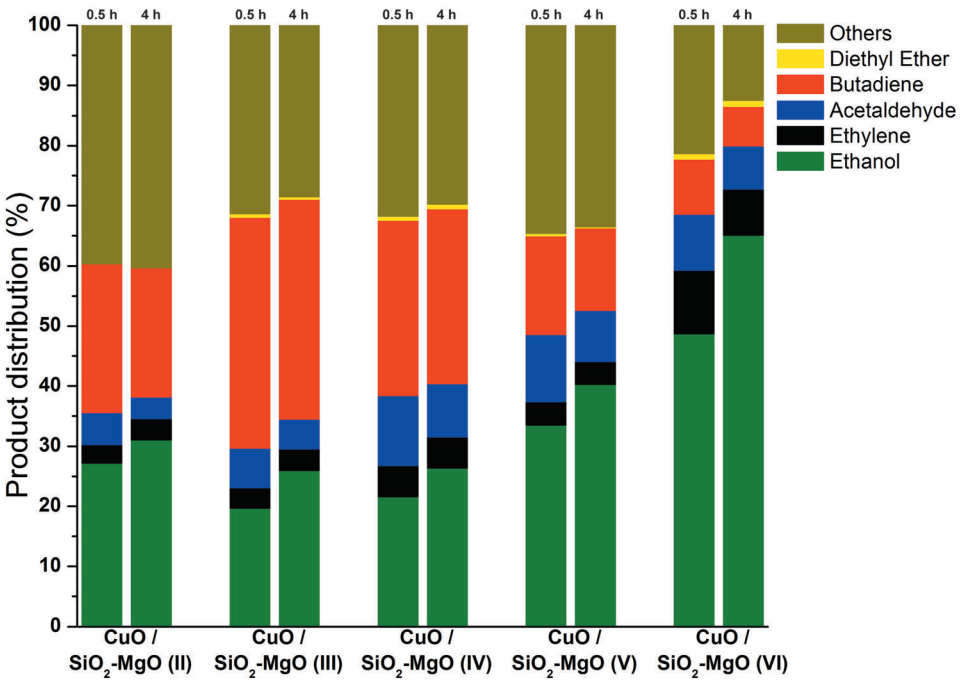

Figure 4. Product distribution for the CuO/SiO_2–MgO catalysts after 0.5 and 4 h on stream. Conditions: 0.2 g catalyst, reaction temperature 698 K, ethanol (gas phase) and nitrogen flow 2 and 98 mL min^{-1}, respectively.

Table 1. Butadiene yield, ethanol conversion, and butadiene selectivity observed for the best SiO_2–MgO and CuO (1 wt%)/SiO_2–MgO catalysts at 698 K tested at the start of the reaction (0.5 h) and after 4 h on stream.

Entry	Catalyst	BD yield [%]		EtOH conversion [%]		BD selectivity [%]	
		0.5 h	4 h	0.5 h	4 h	0.5 h	4 h
1	SiO_2–MgO(III)	17	16	51	52	34	32
2	CuO/SiO_2–MgO(III)	38	37	80	74	48	49

tanol and acetone, C_6-oxygenated compounds were now observed among the main byproducts.

Catalyst characterization

The large variation in catalytic activity of the (CuO-impregnated) SiO_2–MgO catalysts could be correlated with differences in catalyst structure. Considering the commonly proposed mechanisms, and, in particular, the different elementary steps reported, it seems evident that a specific balance between acidic and basic sites is required for selective butadiene production; quite surprisingly, not much is reported in the open literature with respect to the type, strength, and abundance of acidic/basic sites required for a good catalyst material for the Lebedev process. The strength and number of acidic and basic sites on the different catalysts were measured by temperature-programmed desorption (TPD) of NH_3 and CO_2, respectively, whereas overall acidity/basicity was determined using Hammett indicators. Broad desorption peaks are observed by NH_3-TPD for all SiO_2–MgO catalysts, especially for the catalysts prepared through co-precipitation. The number of acid sites varies in the order: SiO_2–MgO (VI) > SiO_2–MgO (V) ≈ SiO_2–MgO (IV) > SiO_2–MgO (III) > SiO_2–MgO (II). This order is in good agreement with the combined amounts of ethylene and diethyl ether byproducts, which are produced through ethanol dehydration on the acidic sites of the catalysts. The significantly increased diethyl ether formation over the two co-precipitated catalysts [and partially over SiO_2–MgO (IV) prepared through wet-kneading] also points at a larger fraction of strongly acidic sites, as also evidenced by a broadening of the NH_3 desorption signal at higher temperatures (not shown).

The basic sites on the different materials were initially probed by using CO_2-TPD, which showed the amount of basic sites to vary in the following order: SiO_2–MgO (II) > SiO_2–MgO (III) > SiO_2–MgO (IV) > SiO_2–MgO (V) > SiO_2–MgO (VI). This order follows inversely the amount of acidic sites as determined by NH_3-TPD, again emphasizing that different preparation methods lead to the presence of different amounts of acidic/basic sites on the catalysts. However, the calculated number of basic sites from the TPD data was unexpectedly low in all cases, that is, about tenfold lower than the number of acidic sites calculated using NH_3-TPD. Given the overall basicity of the materials (see below), this suggests that not all (catalytically) relevant basic sites are properly probed by CO_2 under the applied TPD conditions. Such a discrepancy has been observed before, for instance by Liu and coworkers for MgO–ZrO_2 materials,[23] and requires further study.

The overall acidity/basicity of the different catalysts was assessed using a set of Hammett indicators of increasing pK_a value. If these indicators are protonated or deprotonated by a solid acid/base a color change is observed, which allows for a pK_a range to be determined for the solid materials.[24,25] More specifically, when testing indicators in order of increasing pK_a value, the lower limit of the pK_a value of the catalyst is given by the pK_a value of the last indicator that showed color change (i.e., the indicator for which the initially neutral form was still mainly converted into the deprotonated one) and the upper limit of the catalyst's pK_a value is defined by the first indicator that does not show color change. As expected, the different preparation methods used led to a different overall basicity/acidity for the various SiO_2–MgO catalysts (Table 2). The materials are found to be predominantly basic, with some materials capable of inducing color change in indicators having pK_a values as high as 15.0 (2,4-dinitroaniline). This shows that the total amount of basic sites is actually underestimated by the CO_2-TPD measurements. The order of overall basicity of the catalysts was found to be: SiO_2–MgO (II) ≈ SiO_2–MgO (III) > SiO_2–MgO (IV) > SiO_2–MgO (VI), with the co-precipitated SiO_2–MgO (VI) thus having less acidity than all of the wet-kneaded catalysts. SiO_2–MgO (IV) is the least basic of the wet-kneaded

Table 2. Overview of the different preparations for the SiO_2–MgO catalyst materials, their corresponding BET surface areas, total acidity, and overall basicity.

Sample	Preparation method[a]	Preformed (hydr)oxides	SiO_2 particle size [nm]	S_g [$m^2 g^{-1}$]	Total acidity[b] [mmol g^{-1}]	pK_a range[c]	Comments
SiO_2–MgO (I)	PM	Y	~425				
SiO_2–MgO (II)	WK	Y	~425	124	0.145	15.0–17.2	SiO_2: adding EtOH/NH_3 to TEOS
SiO_2–MgO (III)	WK	Y	30–100	139	0.219	15.0–17.2	SiO_2: adding TEOS to EtOH/NH_3
SiO_2–MgO (IV)	WK	Y	20–40	358	0.234	~15.0[d]	SiO_2: commercial Aerosil 300
SiO_2–MgO (V)	CP	N	~425	156	0.242	n.d.[e]	$Mg(NO_3)_2$ added to TEOS after 20 min
SiO_2–MgO (VI)	CP	N	–[f]	225	0.268	9.3–15.0	$Mg(NO_3)_2$ and TEOS added simultaneously

[a] PM = physical mixture; WK = wet-kneading; CP = co-precipitation. [b] Determined by means of NH_3-TPD. [c] Determined using Hammett indicators. [e] The color observed is between that of the neutral (protonated) and deprotonated forms of 2,4-dinitroaniline (pK_a = 15.0). [f] pK_a could not be determined due to intrinsic coloration of the material. [d] No SiO_2 phase was observed for this catalyst material.

catalysts, showing the influence of the SiO_2 particle size on the acid–base properties.

The acidity/basicity studies suggest that the co-precipitated catalysts [SiO_2–MgO (V) and (VI)] combine an excessive amount of acidic sites with an insufficient amount of basic ones, which results in the high amounts of by-products produced through ethanol dehydration (i.e., ethylene and diethyl ether). This ultimately leads to a poor butadiene yield. Conversely, the large number of basic sites in SiO_2–MgO (II) also leads to a butadiene yield lower than in the case of the other two wet-kneaded catalysts, SiO_2–MgO (III) and SiO_2–MgO (IV). The latter catalysts contain an intermediate amount of both acidic and basic sites, which results in a different product distribution and, eventually, a higher butadiene yield.

Powder X-ray diffraction (XRD) patterns also show clear structural differences as a result of preparation method. As a result of the low copper loading, the XRD patterns for the CuO-containing catalysts (data not shown) are identical to the unpromoted ones (Figure 5). For all catalysts, a halo in the region $2\theta = 20^\circ$–40° is observed due to the presence of amorphous SiO_2.[13,26] Only the WK samples show peaks that could be attributed to the periclase phase of MgO, at $2\theta = 42.9^\circ$, 50.2°, 73.8°, 89.4°, and 94.6°,[27] with the intensity of the periclase peaks varying for the different samples.

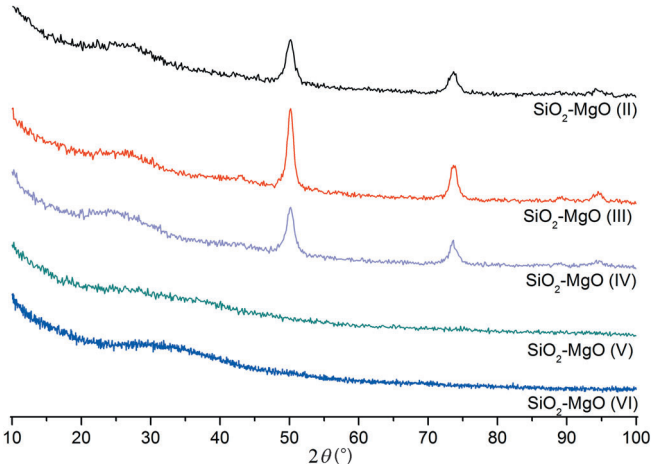

Figure 5. XRD diffractograms of the various SiO_2–MgO catalysts.

The morphology of the various SiO_2–MgO materials that have been reported as active catalysts for the Lebedev process has been little studied. Only Kvisle et al. used TEM to study the morphology of SiO_2–MgO catalysts prepared through wet-kneading.[12] In their case, the single oxides were observed to consist of leaflets (5–10 nm) of SiO_2 and platelets (30–40 nm) of MgO. The wet-kneaded catalysts were shown to contain substantially bigger SiO_2 particles, with the overall morphology consisting of inhomogeneous leaflets and platelets containing both components.

In our case, TEM analysis proved extremely useful as the observed morphological differences could be correlated to catalytic performance. In the PM catalyst (Figure 6a), the MgO platelets and monodisperse, smooth SiO_2 spheres of approximately 425 nm could be clearly distinguished. The lack of intimate contact between the two components is believed to be the main reason of its poor activity. Indeed, both acidic and basic sites are required for a series of elementary steps in the Lebedev process (Scheme 1) and lack of proximity between the different active sites results in the very limited selectivity to butadiene.

The TEM results for samples obtained by WK or CP were quite different. The WK catalysts (II)–(IV) show spherical SiO_2 particles (as expected for the Stöber-like preparation) of variable size that are to different extents covered by or embedded in MgO. SiO_2–MgO (II), for instance, was found to consist of 425 nm SiO_2 spheres and islands of thick platelets of MgO (Figure 6b). However, closer inspection revealed the intimate contact between the phases as a roughening of the surface of the SiO_2 spheres, which are decorated with a thin layer of MgO (Figure 6b1 and b2). The morphologies of SiO_2–MgO (III) and SiO_2–MgO (IV) again showed thick platelets of MgO and MgO-embedded SiO_2 spheres, but the latter are now much smaller (30–100 nm for III and 20–40 nm for IV). As a result of the smaller SiO_2 particles in these two catalysts, the contrast with the MgO component is insufficient to clearly observe MgO layers embedding the SiO_2 spheres. Nevertheless, given the similar preparation method, such layers are expected to play an important role in these two samples as well. The TEM image of CP SiO_2–MgO (V) shows SiO_2 spheres completely covered in a thick MgO layer. The other CP sample SiO_2–MgO (VI) displayed an ill-defined morphology in which neither SiO_2 spheres nor MgO platelets could be identified.

Good butadiene selectivity can thus be correlated to proper intimate contact between the two components; too intimate a contact, as in the CP material SiO_2–MgO (VI), is detrimental for butadiene production, but a (crystalline) MgO layer that embeds the SiO_2 particles, as observed for the WK samples, on the other hand, greatly improves activity and selectivity to butadiene. A thin layer appears to be more advantageous, implying that the best performance is achieved when SiO_2 can still interact with the substrate, but in a way that is mediated by MgO. Large MgO-only areas, such as those observed in SiO_2–MgO (II), probably contribute to ethanol conversion but with lower selectivity to butadiene.

TEM analysis of the CuO-containing catalysts showed that the typical morphologies shown in Figure 6 for the non-impregnated samples are retained upon addition of copper-containing (nano)particles could be seen on any of the samples through bright field or dark field TEM nor by high angle annular dark field scanning transmission electron microscopy (HAADF-STEM). Energy dispersive X-ray (EDX) analysis did show that Cu-containing species can be found at both SiO_2-rich and MgO-rich areas (Figure 6C′1 and C′2). This lack of preference is repeatedly seen on different catalysts and at different areas of the same catalyst.

The fact that no CuO nanoparticles are observed by TEM can either point at an intrinsic lack of contrast with the MgO phase, depending on crystallinity and specific morphology of stacked MgO platelets, at the absence of nanometer-sized CuO particles or at particles or clusters too small to be resolved.

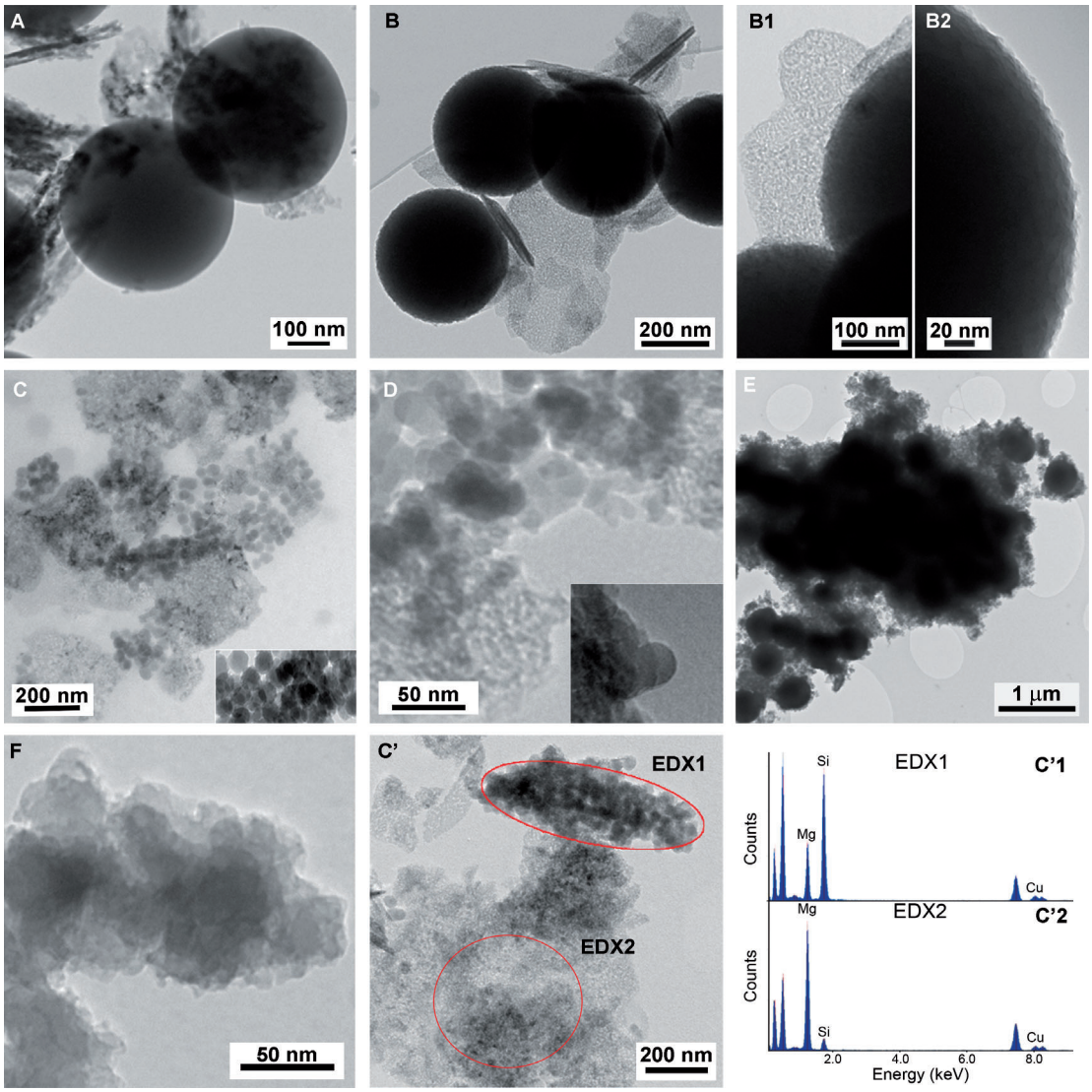

Figure 6. TEM images of A) SiO_2–MgO (I), B) SiO_2–MgO (II), C) SiO_2–MgO (III), D) SiO_2–MgO (IV), E) SiO_2–MgO (V), F) SiO_2–MgO (VI), and C′) CuO (1 wt%)/SiO_2–MgO (III). EDX scan of a C′1) SiO_2-rich region of CuO (1 wt%)/SiO_2–MgO (III) and C′2) of a MgO-rich region of CuO (1 wt%)/SiO_2–MgO (III).

The lack of crystallinity (Figure 5) in the CP samples V and VI seem to discard the former explanation, but an intrinsic impossibility of observing CuO on MgO cannot be completely excluded. Although metallic Cu particles on MgO have been often studied using TEM, we are not aware of any other studies in which the particle size of CuO on MgO was studied using TEM.

Identification of the nature and size of the CuO species is further complicated by the possibility that chemical structures other than CuO nanoparticles or clusters can be formed. El-Shobaky et al.[28] suggested that CuO/MgO solid solutions are formed in CuO-doped MgO catalysts, based on the absence of CuO diffraction peaks in samples containing up to 23 wt% CuO. Solid solution formation was attributed to a thermal treatment performed at 673 K, a temperature that is lower than the one used for calcination of our samples.

To gain further insight into the nature of the CuO species supported on SiO_2–MgO, the samples were also characterized by UV/Vis spectroscopy before and after addition of CuO. The unpromoted SiO_2–MgO catalysts show three characteristic bands at 210, 250, and 290 nm (Figure 7). Coluccia et al.[29,30] previously assigned two similar bands at 230 and 274 nm of MgO to charge transfer between Mg^{2+} and four- and three-coordinated O^{2-} ions, respectively. The latter absorption band at 274 nm was thus thought to correspond to the more unsaturated and more reactive sites on MgO. In our case, the two bands are slightly shifted, yet match the position of the bands measured for pure MgO (data not shown). The 290 nm band is similar for all catalysts, which, therefore, all seem to contain only a small amount of these unsaturated sites; on the other hand, the four-coordinated oxygen CT bands vary both in intensity and position. It is particularly intense in SiO_2–MgO (V) and SiO_2–MgO(III), whereas the intensity is much lower for SiO_2–MgO (VI); this sample is prepared through a pure co-precipitation route and as a result has a lower amount of oxygen atoms coordinated with Mg^{2+} only; this again points at the ab-

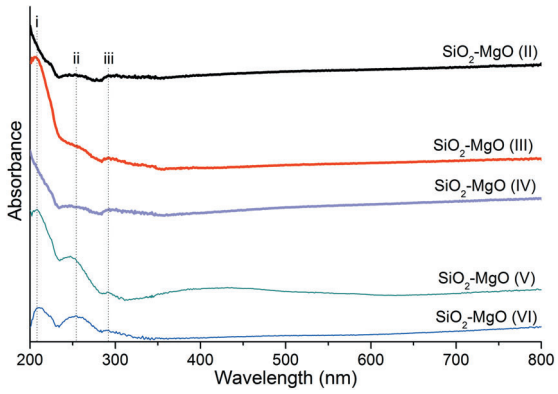

Figure 7. UV/Vis spectra of the SiO_2–MgO samples: i) Mg–O-based charge transfer involving tetra-coordinated oxygen, ii) Mg–O–Si-based charge transfer links, and iii) MgO-based charge transfer involving tris-coordinated oxygen.

sence of an appropriate MgO-like structure in this catalyst, as also observed using XRD and TEM. For SiO_2–MgO (II) and SiO_2–MgO (IV) a shoulder can be observed at approximately 210 nm, whereas an additional band seems to be centered at a wavelength lower than 200 nm.

The band located at around 260 nm was also seen by Kvisle et al.[12] for a wet-kneaded SiO_2–MgO catalyst. It was assigned to Mg–O–Si links based on the observation that the mineral antigorite ($Mg_3(OH)_3Si_2O_5$) has a band at the same position and is known to be active in the Lebedev process. In our case, the intensity of the 250 nm band varies consistent with this assignment, that is, the wet-kneaded samples show only a weak shoulder at ~250 nm, whereas co-precipitated materials, expected to contain a much larger amount of Mg–O–Si bonds, show a much higher absorption at this wavelength. These results again indicate that an optimal catalyst for the Lebedev process requires an intimate contact between the two components but not full mixing of the two (see Figure 3).

The UV/Vis spectra of the CuO-containing samples show two additional transitions (Figure 8): i) a ligand to metal charge transfer band (LMCT) in the region 200–550 nm and ii) d–d transitions seen as a broad band around 700–750 nm for octahedral coper species and as a weak band at ~1380 nm (not shown) for d–d transitions in tetrahedral copper species.

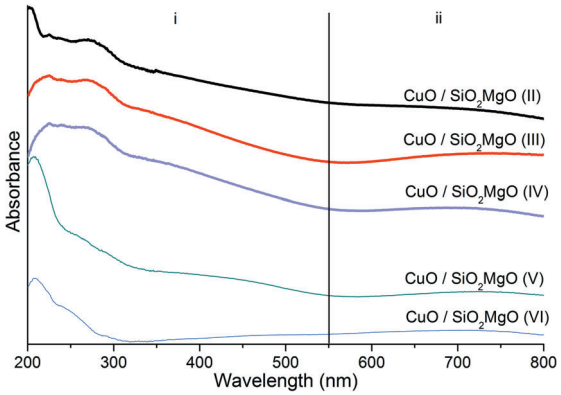

Figure 8. UV/Vis spectra of the CuO/SiO_2–MgO samples before reaction: i) bands assigned to LMCT transitions and ii) bands assigned to d–d transitions.

Neither of these d–d transitions, however, provided further insight into the differences in catalytic performance and nature of CuO. On the contrary, the LMCT bands associated with the CuO species proved insightful for correlating structure to activity. Multiple bands are observed in the 200–300 nm region, corresponding to O^{2-} to Cu^{2+} CT of isolated copper oxide species.[31–33] The presence of such CuO species on both components (as shown by EDX) of the catalyst accounts for the multiple observed features. The position of these CT bands is known to depend on the type and morphology of the supports and the procedure employed to support CuO.[33–35] Kong et al., for instance, observed variations in the position and intensity of CT bands of isolated CuO species for CuO/SBA-15 and CuO/KIT-6.[36] Bravo-Suárez et al. recently reported two different bands centered at 260 and 360 nm for CuO/$MgAlO_x$ mixed oxides.[37] The 260 nm band was assigned to an LMCT of isolated octahedral Cu^{2+}–O^{2-} species, whereas the latter band was attributed to the presence of oligomers of the type Cu–O–Cu. Derrien and co-workers[38] reported a band at 235 nm for CuO supported on mesoporous SiO_2 spheres, whereas Shimokawabe et al.[32] reported the same band to be at 270 nm for CuO supported on SiO_2, which illustrates the additional dependence on morphology.

Moreover, the weak shoulder in the region 300–550 nm (Figure 8), assigned to LMCT in cluster-like species (Cu–O–Cu), is found to vary strongly for our CuO/SiO_2–MgO materials, being highest in intensity for the WK catalysts, SiO_2–MgO(III) and SiO_2–MgO(IV) in particular. Only in SiO_2–MgO(VI), which gives the lowest butadiene yield, it is completely absent. The fact that the two WK catalysts SiO_2–MgO(III) and SiO_2–MgO(IV) are more active and more selective towards butadiene formation suggests that these cluster-like CuO species promote butadiene formation. This is tentatively explained considering that the formation of acetaldehyde molecules on different sites in close proximity with each other could make their condensation (proposed by some authors to be the rate-limiting step of the complete process)[12,22] easier than on isolated CuO species, thus leading to cascade reactions for the formation of 3-hydroxybutanal, crotonaldehyde, and crotyl alcohol, all known to be key intermediates in the Lebedev process.

Conclusions

SiO_2–MgO mixed oxides have often been reported as most efficient catalyst materials for the one-step conversion of ethanol to butadiene. However, the reason as to why this combination of oxides is so selective towards the production of butadiene remains elusive. A better understanding of the influence of preparation method and promotion on activity and selectivity is needed for the design of better catalysts for the Lebedev process.

We observed a clear effect of the synthesis method of SiO_2–MgO on morphology, acidity, and basicity. More specifically, all catalyst materials prepared by wet-kneading proved to be more active and selective towards butadiene, which points at

the importance of the thin layer of MgO embedding the SiO2 spheres and the specific local structure obtained through this preparation method. Decreasing the size of these SiO_2 spheres further improved the selectivity towards butadiene production.

In addition, the introduction of a small amount of CuO as promoter is shown to bring about a significant improvement in both total ethanol conversion and butadiene yield, resulting in a butadiene selectivity of around 53%; the added CuO increases acetaldehyde production, effectively shifting the rate-determining step of the process.

The different preparation methods lead to significant differences in the amount of acidic and basic sites. The large amounts of by-products formed by ethanol dehydration over the co-precipitated catalysts can be directly related to the high acidity of these materials. The wet-kneaded SiO_2–MgO catalysts are more basic, with the exact acidity/basicity depending on the size of the SiO_2 spheres, with smaller SiO_2 spheres providing the best balance of basic and acidic sites.

UV/Vis studies provided further insights into the nature of the catalyst materials, that is, in the extent of intimate mixing of the SiO_2 and MgO phases and into the type of CuO species deposited and responsible for the increased butadiene yields. Although CuO nanoparticles could not be seen by our TEM analysis, Cu is present on both phases of the catalyst and small cluster-like CuO species are proposed to have a positive impact on butadiene formation. The results reported here thus provide new insights into the structural characteristics required for a good catalyst for the Lebedev process.

Further studies are now required to disclose more details on the exact nature of acidic/basic active sites required for butadiene production and on the nature, location, and temporal behavior of the CuO promoter. Together with the results presented herein, this will result in a more complete structure–activity relationship and ultimately in improved methods for the synthesis of efficient Lebedev catalysts.

Experimental Section

Materials

Davicat Si 1404 silica from Grace and Aerosil 300 silica by Degussa were used as purchased and without further treatment. $Mg(NO_3)_2\times 6H_2O$ (99+%, Acros), $Cu(NO_3)_2\times 3H_2O$ (99%, Acros), and tetraethyl orthosilicate (TEOS, 98%, Aldrich) were employed for the preparation of the different oxides. NH_3 (25%, Merck) and ethanol (100%, Interchema) were used during synthesis. Benzene (Sigma–Aldrich, ACS reagent ≥99.0%) was used for the Hammett indicator study.

Catalyst preparation

Six SiO_2–MgO [denoted (I)–VI] catalysts (all with molar ratio 1:1) were prepared in different ways to investigate the effect of preparation method on catalytic performance. SiO_2–MgO (I) was a physical mixture (PM) prepared by mixing the two calcined individual components, prepared as detailed below, for 10 min in a mortar. MgO was prepared by dissolution of the nitrate precursor in water (0.5 M), followed by dropwise addition of a 1 M aqueous NH_3 solution to precipitate the corresponding hydroxide ($Mg(OH)_2$). The precipitate was aged overnight, washed several times with deionized water and recovered through centrifugation, dried at 393 K, and finally calcined in stagnant air at 773 K for 5 h. A modified Stöber route was used for the preparation of SiO_2. TEOS was hydrolyzed using an ethanol–NH_3 solution (5:1 *v/v*) at room temperature for 24 h. After washing with ethanol, SiO_2 was dried and calcined as described for the other oxides.

The samples SiO_2–MgO (II-IV) were synthesized by a wet-kneading (WK) technique similar to the one reported by Kvisle et al.[12] The two uncalcined components (molar ratio of 1:1) were mixed at room temperature for 4 h in water; in all cases $Mg(NO_3)_2\times 6H_2O$ was employed as precursor and the corresponding hydroxide was obtained as described before. For catalyst SiO_2–MgO (II), the SiO_2 component was prepared using the modified Stöber route described above. For catalyst SiO_2–MgO (III), the SiO_2 component (final concentration is 0.34 M) was prepared by addition of the desired amount of TEOS (17.3 g) at once to an ethanol–NH_3 solution in a closed vessel, followed by aging at 308 K overnight; the material was subsequently dried in a rotary evaporator at 328 K. SiO_2–MgO (IV) was prepared by WK using Aerosil 300 silica (Degussa).

The catalysts SiO_2–MgO (V) and (VI) were prepared by co-precipitation (CP) methods: in the case of SiO_2–MgO (V) an EtOH/NH_3 = 5:1 (*v/v*) solution (240 mL) was added at once to the desired amount of TEOS (approximately 2.6 g). After 20 min, $Mg(NO_3)_2$ (approximately 3.2 g) dissolved in 200 mL of ethanol was added to the previous solution. SiO_2–MgO (VI) was prepared through addition of 240 mL of ethanol–NH_3 solution (5:1 *v/v*) to the same amounts of the two precursors dissolved in 200 mL of ethanol.

For all the SiO_2–MgO samples, the precipitate was washed several times with deionized water and recovered through centrifugation, dried at 393 K, and then calcined at 773 K for 5 h.

CuO (1 wt%) was supported on SiO_2–MgO (II)–(VI) by IWI (incipient wetness impregnation). 0.1 mL of a 0.63 M solution of $Cu(NO_3)_2\times 3H_2O$ in water was added to the support material (previously dried for 1 h at 353 K) and, once the impregnation was completed, the sample was left for 1 h to equilibrate, then dried for 12 h under vacuum at RT, and finally, calcined at 773 K for 5 h.

Catalyst testing

For all catalytic tests, quartz wool was placed in a U-shaped quartz reactor, before addition of the catalyst (0.2 g; sieved to 425–90 μm particle size). The desired amount of ethanol was fed through a Bronkhorst CEM system consisting of three parts: a liquid flow controller to check the amount of ethanol fed, a gas flow controller for the nitrogen used as carrier gas, and finally, a mixing chamber kept at 303 K where the gaseous mixture was formed and fed downstream into the reactor. The total flow used was 100 mL min^{-1}, of which 2 mL min^{-1} consisted of ethanol in the gas phase. Reactions were run at 698 K. The analysis of the reaction mixture was performed by means of GC-FID (gas chromatography with flame ionization detector) using a CP poraplot Q-HT column; quantification of the main components (ethanol, ethylene, acetaldehyde, butadiene, and diethyl ether) was based on calibration curves obtained by feeding known amounts of the various compounds. The following definitions were used (mol: moles of observed substance:

Ethanol conversion:

$$X_{EtOH}(\%) = 100 \times \frac{mol_{EtOH\ converted}}{mol_{EtOH\ initial}}$$

Yields:

$$Y_i(\%) = 100 \times \frac{\mathrm{mol}_{\mathrm{product\ i}}}{\mathrm{mol}_{\mathrm{EtOH\ initial}}}$$

Selectivity of the i-main component:

$$S_i(\%) = 100 \times \frac{\mathrm{mol}_{\mathrm{product\ i}}}{\Sigma \mathrm{mol}_{\mathrm{product\ i}}}$$

Catalyst characterization

TEM images of the SiO_2–MgO samples were obtained on a Tecnai 12 apparatus operated at 120 keV. The catalyst particles were deposited on a TEM grid and analyzed as received. The CuO-containing catalysts were imaged on a Tecnai F20 apparatus operating at 200 keV and equipped with an EDX detector. Nickel grids were used for the EDX study of CuO-containing samples.

Textural properties of the materials were studied by nitrogen physisorption measurements at 77 K using a Micromeritics Tristar 3000. Prior to the adsorption measurements the samples were dried at 573 K for 12 h. The Brunauer–Emmett–Teller (BET) method was applied to calculate the total surface area. The *t*-plot method was applied to obtain the micropore volume and external surface area. The Barrett–Joyner–Halenda (BJH) model was used to determine the size of the mesopores.

XRD patterns were obtained by using a Bruker-AXS D2 Phaser powder X-ray diffractometer using $CoK_{a1,2}$ with $\lambda = 1.79026$ Å, operated at 30 kV. Measurements were carried out between $2\theta = 10^\circ$ and 100° using a step size of 0.05° and a scan speed of $0.5^\circ\ s^{-1}$. UV/Vis spectra were collected using a Varian Cary 500 UV/Vis/NIR spectrometer equipped with a diffuse reflectance spectroscopy (DRS) accessory. The spectra were collected between 200 and 800 nm with a data interval of 1 nm and at a rate of 600 nm min^{-1}. NH_3-TPD measurements were performed on a Micromeritics ASAP2920 apparatus. Typically, the sample (0.2 g) was placed in a quartz reactor. The samples were dried in the apparatus in a helium flow by heating with a temperature ramp of 5 K min^{-1} to a maximum temperature of 873 K. Subsequently, the sample was cooled to 373 K; at this point, NH_3 pulses of 25.31 cm^3 min^{-1} were applied. The sample was then heated to 873 K with a ramp of 5 K min^{-1} to induce desorption of NH_3. A procedure similar to the one described for NH_3-TPD was employed in the case of CO_2-TPD, the main difference being the lower temperature (313 vs 373 K) at which CO_2 pulses were fed to the sample. For the calculation of the number of acidic or basic sites, it was assumed that only one molecule of NH_3 or CO_2 could adsorb on a single site.

For the Hammett indicator study, benzene was dried over molecular sieves and stored under an argon atmosphere. All experiments were performed using standard Schlenk techniques. A solution of each indicator was prepared by dissolving a specific indicator (25 mg) in dry benzene (25 mL). The six indicators used were (in order of increasing pK_a): bromothymolblue (ABCR, p$K_a = 7.2$), phenolphtalein (Sigma–Aldrich, ACS reagent, p$K_a = 9.3$), 2,4-dinitroaniline (Acros Organics, 99%, p$K_a = 15.0$), 4-chloro-2-nitroaniline (Sigma–Aldrich purum, $\geq$98% (HPLC), p$K_a = 17.2$), 4-nitroaniline (Acros Organics, 99%, p$K_a = 18.4$), and 4-chloroaniline (Sigma–Aldrich, 98%, p$K_a = 26.5$). Before each experiment, the catalyst (0.1 g) was dried at 473 K in vacuum. The flask containing the catalyst was then put under argon atmosphere, after which 2 mL of dry benzene were added to the sample under investigation; at this point a few drops of the indicator solution (in the protonated, neutral form) were added to the suspension of the catalyst in benzene. After a few minutes, a color change was observed on the surface of the solid catalyst, indicating that the majority of the indicator was converted into its deprotonated form. The flask was then stored for 24 h to confirm the color change (or its absence).

Acknowledgements

This project has been performed in the framework of the Catch-Bio program. The authors gratefully acknowledge the support of the Smart Mix Program of the Netherlands Ministry of Economic Affairs and the Netherlands Ministry of Education, Culture and Science.

Keywords: butadiene · copper · ethanol · heterogeneous catalysis · silica–magnesia

[1] J. J. Bozell, G. R. Petersen, *Green Chem.* **2010**, *12*, 539 – 554.
[2] S. González-García, L. Luo, M. T. Moreira, G. Feijoo, G. Huppes, *Biomass Bioenergy* **2012**, *36*, 268 – 279.
[3] R. P. John, G. S. Anisha, K. M. Nampoothiri, A. Pandey, *Bioresour. Technol.* **2011**, *102*, 186 – 193.
[4] C. Angelici, B. M. Weckhuysen, P. C. a Bruijnincx, *ChemSusChem* **2013**, *6*, 1595 – 1614.
[5] W. C. White, *Chem.-Biol. Interact.* **2007**, *166*, 10 – 14.
[6] P. C. A. Bruijnincx, B. M. Weckhuysen, *Angew. Chem. Int. Ed.* **2013**, *52*, 11980 – 11987; *Angew. Chem.* **2013**, *125*, 12198 – 12206.
[7] J. Ostromisslenski, *J. Russ. Phys. Chem. Soc.* **1915**, *47*, 1472 – 1506.
[8] S. V. Lebedev, Br. Pat. 331,402, **1929**.
[9] S. V. Lebedev, *J. Gen. Chim.* **1933**, *3*, 698 – 708.
[10] S. K. Bhattacharyya, S. K. Sanyal, *J. Catal.* **1967**, *7*, 152 – 158.
[11] H. Niiyama, S. Morii, E. Echigoya, *Bull. Chem. Soc. Jpn.* **1972**, *45*, 655 – 659.
[12] S. Kvisle, A. Aguero, R. P. A. Sneeden, *Appl. Catal.* **1988**, *43*, 117 – 131.
[13] E. V. Makshina, W. Janssens, B. F. Sels, P. A. Jacobs, *Catal. Today* **2012**, *198*, 338 – 344.
[14] R. Ohnishi, T. Akimoto, K. Tanabe, *J. Chem. Soc. Chem. Commun.* **1985**, 1613 – 1614.
[15] M. D. Jones, C. G. Keir, C. Di Iulio, R. a. M. Robertson, C. V. Williams, D. C. Apperley, *Catal. Sci. Technol.* **2011**, *1*, 267 – 272.
[16] W. J. Toussaint, J. T. Dunn, D. R. Jackson, *Ind. Eng. Chem.* **1947**, *39*, 120 – 125.
[17] G. Natta, R. Rigamonti, *Chim. Ind.* **1947**, *29*, 195 – 201.
[18] Y. Kitayama, M. Satoh, T. Kodama, *Catal. Lett.* **1996**, *36*, 95 – 97.
[19] A. D. Patel, K. Meesters, H. den Uil, E. de Jong, K. Blok, M. K. Patel, *Energy Environ. Sci.* **2012**, *5*, 8430 – 8444.
[20] F.-W. Chang, H.-C. Yang, L. S. Roselin, W.-Y. Kuo, *Appl. Catal. A* **2006**, *304*, 30 – 39.
[21] N. Takezawa, C. Hanamaki, H. Kobayashi, *J. Catal.* **1975**, *38*, 101 – 109.
[22] W. M. Quattlebaum, W. J. Toussaint, J. T. Dunn, *J. Am. Chem. Soc.* **1947**, *69*, 593 – 599.
[23] S. Liu, X. Zhang, J. Li, N. Zhao, W. Wei, Y. Sun, *Catal. Commun.* **2008**, *9*, 1527 – 1532.
[24] Y. Ono, H. Hattori, *Solid Base Catalysis*, Springer, **2011**.
[25] J. Take, N. Kikychi, Y. Yoneda, *J. Catal.* **1971**, *21*, 164 – 170.
[26] R. Brambilla, C. Radtke, J. H. Z. dos Santos, M. S. L. Miranda, *Powder Technol.* **2010**, *198*, 337 – 346.
[27] J. C. A. A. Roelofs, J. A. van Bokhoven, A. J. van Dillen, J. W. Geus, K. P. de Jong, *Chem. Eur. J.* **2002**, *8*, 5571 – 5579.
[28] G. A. El-Shobaky, M. N. Hamed, F. F. Abdalla, S. A. El-Molla, *Colloids Surf. A* **2002**, *207*, 293 – 301.
[29] S. Coluccia, A. J. Tench, R. L. Segall, *J. Chem. Soc. Faraday Trans.* **1979**, *75*, 1769 – 1779.
[30] S. Coluccia, A. Barton, A. J. Tench, *J. Chem. Soc. Faraday Trans.* **1981**, *77*, 2203 – 2207.

[31] K. V. R. Chary, K. K. Seela, G. V. Sagar, B. Sreedhar, *J. Phys. Chem. B* **2004**, *108*, 658 – 663.
[32] M. Shimokawabe, N. Takezawa, H. Kobayashi, *Appl. Catal.* **1982**, *2*, 379 – 387.
[33] S. Velu, K. Suzuki, M. Okazaki, M. P. Kapoor, T. Osaki, F. Ohashi, *J. Catal.* **2000**, *194*, 373 – 384.
[34] H. Praliaud, S. Mikhailenko, Z. Chajar, M. Primet, *Appl. Catal. B* **1998**, *16*, 359 – 374.
[35] Z. Wang, H. Wan, B. Liu, X. Zhao, X. Li, H. Zhu, X. Xu, F. Ji, K. Sun, L. Dong, Y. Chen, *J. Colloid Interface Sci.* **2008**, *320*, 520 – 526.
[36] A. Kong, H. Wang, X. Yang, Y. Hou, Y. Shan, *Micropor. Mesopor. Mat.* **2009**, *118*, 348 – 353
[37] J. J. Bravo-Suárez, B. Subramaniam, R. V. Chaudhari, *J. Phys. Chem. C* **2012**, *116*, 18207 – 18221;
[38] G. Derrien, C. Charnay, J. Zajac, D. J. Jones, J. Rozière, *Chem. Commun.* **2008**, 3118 – 3120.

Received: April 29, 2014
Published online on July 14, 2014